I. Introduction

Applications and resource estimates for open system simulation on a quantum computer

Evgeny Mozgunov^{1,2}

¹Center for Quantum Information Science & Technology, University of Southern California ²Department of Electrical & Computer Engineering, University of Southern California

We study applications of a fully controllable open system quantum simulator. A universal quantum computer can realize such a simulator, and some classical methods can also approximate it. We introduce two concrete computational problems, such that finding their solution would have direct scientific or industrial utility. The scientific utility is exemplified by a computation of nonequilibrium behavior of Ca₃Co₂O₆, which has been studied in the costly MagLab experiments. Specifically, an order of \$2M per material can be saved if an affordable quantum computer simulation is used to screen the materials before sending them to MagLab. For industrial utility, we develop a methodology that allows researchers of various backgrounds to estimate the economic value of an emerging technology consistently. We then apply our approach to the applications of materials with a Metal-Insulator Transition. These materials have not been used commercially yet, but many potential applications, including alternative transistors, neuromorphic computing, and smart windows, amount in total to \$20M for the entire material search performed on a quantum computer. We provide zeroth-order resource estimates for both algorithms on superconducting qubit hardware, finding that simulating long-lifetime nonequilibrium effects presents a new challenge for quantum simulators. Finally, we introduce planted solution problems and their obfuscated versions to test the capabilities of the future quantum device. The intended use of those problems is to match the size of application benchmarks so that solving one guarantees the ability to solve the other.

1

CONTENTS

I. INTRODUCTION

П.	Utility A. Scientific utility: funding B. General methodology for industrial utility C. MagLab single material \$ cost D. Metal-Insulator transition material search \$ cost E. Gibbs state preparation: most likely targets	2 2 2 4 4 5
III.	Problem Statement A. MagLab's application problem (Ca ₃ Co ₂ O ₆) B. Metal-Insulator transition material search application problem	6 6 7
IV.	Quantum Implementation A. Lindbladian QSP	8 9
V.	Resource estimation for proposed quantum algorithms A. Abstract Logical 1. Lindbladian QSP 2. Block encoding for a Lindbladian B. Compiled Logical C. Physical	9 9 9 9 10 11
VI.	Acknowledgments	12
	References	12
A.	Planted solution problems 1. Closed system: Integrable models and T-gates 2. Open system	13 13 14

We study applications of an open system quantum simulator. Such a simulator can be realized by a universal quantum computer [1], and some classical methods can approximate it as well. Our goal is to introduce a concrete computational problem such that finding its solution would have direct scientific or industrial utility. We find an example of the scientific utility to be the investigation of materials that are already studied in high-cost experiments. 20-30 new material samples per year are not understood by low-cost experimental and computational means and are sent to the Magnetic Field Laboratory (MagLab) [2]. These experiments often observe unexplained nonequilibrium phenomena, exemplified by the behavior of $Ca_3Co_2O_6$ [3]. We use them as application instances.

For industrial utility, we focus on material searches. A successful example of a large throughput material search is the search for material for good thermoelectric devices, happening under the umbrella of the Materials Project[4]. There are already commercial applications for those devices, but wide adoption is still dependent on the discovery of better materials and designs using the semi-automated search methodology. The utility of this computational search comes from accelerating their adoption and the projected big markets for applications. Unfortunately for quantum computers, we believe the bottlenecks in this search are largely classical, and most questions can and should be answered using cheaper state-of-theart classical algorithms. Drawing inspiration from the success of these classical techniques, we envision a similar search in the domain of strongly correlated materials. There, classical methods fail, though there are some promising new results [5]. The commonly mentioned applications for these materials include high-temperature superconductivity and metalinsulator transition. The latter is especially suited for an open system study, as one of the central observables is the transport coefficient. It can, in principle, be estimated in a closed system setting, yet we believe the most efficient quantum algorithm for transport contains an open system quantum simulator. The corresponding economic impact will be outlined below.

We also note that many other application instances covered in companion publications, while not directly related to open systems, have their solution by quantum algorithms relying on an unproven assumption of the existence of a high overlap initial state. Estimating that overlap is a challenge, and here we note that for open system thermal state preparation relevant to most condensed matter and material science applications, as well as in quantum chemistry such as surface chemistry, the estimate can be performed under very mild assumptions compared to other state preparation methods.

In Sec. II, we discuss our general metodology of utility estimation and apply it to cases of interest. Then in Sec III we state two of the cases of interest as fully specified mathematical problems. We list available quantum algorithms in Sec. IV, before describing implementation of the best of them for our problems in Sec. V, calculating zeroth order estimates to both logical and physical required resources. Finally, in App. A we use toy problem benchmarks where we can compute the answer to test the capabilities of the future quantum device. The intended use of those planted solution benchmarks is to match the size of the application benchmarks so that solving one guarantees the ability to solve the other.

II. UTILITY

There are two approaches to the utility of scientific findings: to look into the funding science receives and to look into the market of inventions enabled by the discovery in question. The latter is only possible in hindsight, while the former may be insensitive to differences between fundamental and applied research. In an efficient market, one would expect both estimates to result in a similar order of magnitude.

We note that the quantum computer is not necessarily the only way to accomplish the research agenda we outline. Whether it would be accomplished by classical computation, experiment, quantum computer, or a combination of those approaches, the utility is unchanged. In particular, the presence or absence of quantum advantage should not affect our estimate of utility. Nonetheless, we focus on the problems that promise a quantum advantage as well. Below, we will outline the methodology of each approach and attempt both approaches for the chosen application instances.

A. Scientific utility: funding

For the funding estimate, we look into the amount of money spent on solving the problem in question or a problem of equivalent size and significance. The rationale for that is that one capable of solving the problem should be able to negotiate for that amount of remuneration, at least in principle. We note that a transaction like that would not necessarily occur. For example, the creators of AlphaFold did not monetize it in a

way commensurate with the amount of money regularly spent on protein structure experiments and simulations. Possibly, the publicity it generated was of equivalent value to them, and it undoubtedly accelerated biological research, so we believe estimating its value is still appropriate using our methodology even if the hypothetical transaction did not take place.

B. General methodology for industrial utility

The argument that the particular technology's market size is the utility of further research into it is very common. Almost any research is conventionally justified in that way, no matter how distant it is from applications. We would like to challenge this way of thinking by proposing a methodology that would result in a consistent (within 1-2 orders of magnitude) estimate of utility even when applied by different researchers and decision makers independently. While it is true that it is sometimes impossible to trace the influences of fundamental research on applications far in the future, most of the revolutionary technologies of the past have had clear conditions for their discovery. We choose to focus on concrete links between research and applications. Thus, only the research that is part of a clearly defined roadmap to an improvement in the corresponding technology will be assigned nonzero utility in this approach. In this way, we will estimate the effort required for the successful completion of that roadmap and assign the utility to that.

To apply our proposed methodology to quickly and consistently estimate the industrial utility of a particular research program, three pieces of information about it are required:

- 1. A clear roadmap incorporating the solution of the research problem into the design of the product
- A scientific review listing competing technologies for this type of product
- 3. A market report on the size of the market (sum of yearly revenue) of competing products

We will now describe how to utilize each of those sources.

a. Scientific review The risk associated with new technology is that it will not reach the specifications required for mass adoption and, instead, be outmatched by competitors relying on different technologies. In this way, various research directions race against each other in terms of performance metrics. Such performance metrics for different technologies can usually be found in a contemporary scientific review. At the early stages of the race, we choose to divide the utility estimate in a way weighted by the performance metrics, such that the most promising candidates correspond to the larger share of utility. Since the performance metrics vary across fields, and both logarithms and the value itself are being used, we need to set up a unified way to assign those weights. The simplest way is to order n competitive technologies by how promising they are and assign weights $\sim n, n-1...1$ to them. The utility of each technology will then be =weight·utility of the application.

Our approach may fail in more complex situations such as when one of the technologies has already received mass adoption. In that case, while there is a probability that the entire industry will switch to a new technology, complete switches like that are rare. E.g., no one is building coal plants in the US anymore, but the existing ones are still in use, and sometimes their operation is even extended beyond the planned closure date. The switch may not be complete and will have a lot of inertia. The available data does not allow us to reliably estimate this switch probability - indeed, it is hard to formulate a methodology that will result in the same (within 1-2 orders of magnitude) estimate when applied independently by different analysts or research groups. Instead, we rely on a more tangible picture that the new technology will occupy a niche of the market where it is especially advantageous.

b. Market report The data for such market segmentation is usually available in the industry reports published by consulting companies. Those reports can be rather controversial, such as the trillion-dollar estimates of the utility of quantum computers themselves. Below, we outline the methodology we use to interpret those reports, as well as the precautions that need to be taken when using them.

The market size of a technology is commonly estimated as the sum of the yearly revenue of the companies utilizing that technology. More specifically, if a small part of a big company is using it, the corresponding share is used. The revenue is the product of the product's price and the number of sales. We note that technology is definitely not enough to create a product; one also needs people and assets, as well as various other costs. While a company cannot fill the market in question without the corresponding technology, it would not be accurate to count the entire revenue as the utility of the technology. The founder who discovers the technology either invests his own money or seeks venture funding by selling shares of the company when the company is created. Only with that money can the company fill the market. Since there are various monetary figures at various stages of this process, and the revenue itself grows with time, we need a standardized method to reduce it all to a single number - utility. Note that the first stage of venture funding usually values the company relatively cheap, no matter how good the underlying technology is. We see that as the tradition of venture capital and not as the true value of the corresponding technology. We believe that the true value of technologies shows itself in acquisition events, where a big company acquires promising ideas before they become competitors. We also note that for utility estimates, the total revenue is less important than the relative increase with or without the technology. Ideally, that can be computed from the business model and an estimate of how much the technology improves the product. That being said, none of those numbers can easily be used in a unified framework, as they are rarely available. For simplicity, we will assign a factor between 10 (technology will lead to an explosive growth of the business) and 1/10 depending on how central the technology is for the business model. For example, if energy is the leading cost and improvement in efficiency directly translates to energy savings, such as for nitrogen fixation, we choose the factor 1/2. A more detailed estimate of that factor would be as

follows: first, we assume a simple model of seller optimizing profit, and the number of sales n depending linearly on price as $n = n_0 - ep$, where e is the elasticity of demand. The result of profit optimization for production costs c1 and c2 is that the difference in revenue is $r_2 - r_1 = \frac{1}{2}e(c_1 - c_2)$. As the fertilizer market is tied with the population and the arable land, we can estimate elasticity as the remaining need for fertilizer divided by the current price since, at zero price, only the amount needed for current land and population would be purchased. The amount of fertilizer needed would remain approximately the same over a 10-year span. Finally, we estimate lower production costs c_2 from the energy consumption to fix nitrogen. Various methods have O(1) difference in energy cost per unit of mass of nitrogen fixed, so we can expect a novel method to have of order 50% improvement. If it is only a 1% improvement, the estimate can be updated by directly multiplying the factors. Assuming the 50% energy savings, prices close to the production cost, and elasticity $\sim n_0/\text{current}$ price, this estimate results in a factor 1/2 improvement in revenue for the new nitrogen fixation technology.

In contrast, a slightly better product requiring a lot of investment into switching the manufacturing process completely would have two competing effects: rising production costs would lower the revenue, yet the improvement in product quality would increase the revenue, though the effect may be quite complex to formulate. For example, consider thermoelectric devices. While they are sold commercially today, the market is small, mostly consisting of niche cooling applications. The main application of recycling heat is mostly unrealized. It is believed that improvements in efficiency (essentially, the percentage of heat recycled) would make it viable and result in mass adoption. More specifically, the efficiency, together with other figures of merits involving lifespan, production, and maintenance cost of the thermoelectric device, determines the viability for various use cases. The demand in each use case would discontinuously jump from zero to mass adoption, but if one adds these jumps for all use cases, one could approximate the number of sales as linear in the figures of merit. Using the formalism above, that would be $n_0 = aZT$. The change in revenue would then be $en_0a(ZT_2-ZT_1)$. If one expects a tenfold increase in the number of sales, that would roughly translate to a tenfold increase in revenue, assuming other coefficients are O(1). That illustrates that technologies with a small existing market can have much higher utility than the current or projected market size suggests. This applies only to conventionally impossible tasks, e.g. the profitable heat recycling is essentially impossible with the current technology, therefore the existing market is not a good estimate for the potential market. For most technologies, however, the task is already accomplished by the older generation of technology, and the shift in demand is not as dramatic, no matter how good the new generation of technology is.

A related question is, at what time should we take the revenue? With the quantum computer application in mind, we need to wait for at least ten years before the solution to the problem becomes available. Most projections of the market size stop at the 10-year time horizon. Thus, we will use an

estimate of the market size ten years in the future (year 2034) corresponding to the emerging technology or competing technology in case the market is already occupied by existing technology. Unfortunately, the market breakdown based on emerging technologies is not commonly found in consulting reports. At best, we can narrow it down to the niche of the existing technology to be replaced. What is common is another type of estimate: instead of looking at the revenue of the seller of the technology, a report would look at the revenue of all the potential buyers of the technology. Then, the report would note that an improvement in the product would generate some arbitrary fraction, such as a 1%-9% increase in the revenue of the buyers. The possibility of such an improvement is confirmed by experts in the buyers' corresponding businesses. Thus, the total value is computed as a sum of 1%-9% of the revenues of all buyers, and the resulting number for some of the future technologies, such as AI or quantum computing, is quoted in the trillions. An immediate objection is that the revenue of the current semiconductor industry is just \$500b global and \$80b in the US. If they really had a trillion dollar value, they would have been able to increase their revenue correspondingly. Indeed, the consulting message for the semiconductor industry is that they only capture 20% of the value their product generates, and it is the goal for the CEOs of the hardware companies to increase that ratio for future hardware markets, such as specialized AI hardware. For our purposes, we will only look at the value the seller companies were able to realize as revenue, not the optimistic possibility that is quoted in the more controversial reports. Moreover, only when a company based in one country can, in principle, take over the entire global market with a superior technology that cannot be reverse-engineered we use the global revenues instead of the revenue of companies based in one particular country.

A final caution is that a "buzzword" technology attracts scam artists. As a result, only scam industry reports can be found for the current market revenue of some "buzzword" technologies. For example, looking for the market size of neuromorphic devices, one only finds scam reports. A wellknown consulting company's reports are available for the dedicated AI hardware but not for the neuromorphic devices. They likely have not generated enough revenue to report. If we aim to replace dedicated AI hardware with neuromorphic devices, we will need to use the dedicated AI hardware market size and estimate the probability of the switch in some way. The estimate of the market size of a segment like that may vary by two orders of magnitude between reports. Whenever possible, we average the reports of well-known consulting companies, thus achieving one order of magnitude error. As the other factors we used are ad hoc, this estimate would result in two orders of magnitude error. The formula is as follows:

Utility = weight of tech.
$$\times$$
 share in revenue \times (1)

$$\times$$
 global market size of niche tech. (2)

We expect the two utility estimates (science funding and market size) to match within the two orders of magnitude error.

C. MagLab single material \$ cost

LANL's MagLab pipeline contains costly experiments with high magnetic fields. The cost of that pipeline is known (\$39M a year is the budget of MagLab), and it is also known that there is a quantum-classical separation in a $Ca_3Co_2O_6$ experiment [3] proposed as a benchmark. The open system contribution to the dynamics of that benchmark is likely to be important for reproducing the experimental behavior and eventually replacing the experiment altogether.

In our case, the utility would be the MagLab budget divided by the number of materials going through it, thus about \$2M per material.

The specific experiment concerning the nonequilibrium spin states does not have direct applications. In general, spin materials are studied for the advancement of:

- Next-gen storage and computing (especially QC hardware)
- · Magnetoelectrics, piezomagnets, sensors
- Superconductors

While $Ca_3Co_2O_6$ itself is used in prototypes of fuel cells at room temperature and zero magnetic field [6], a concrete application for its low-temperature high field behavior has not been invented. We conclude the market size estimate at \$0 according to our methodology.

D. Metal-Insulator transition material search \$ cost

In this section, we discuss the utility of a material search for the new materials with Metal-Insulator Transition (MIT). First of all, we note that this transition happens at room temperature, so it may be possible to predict it ab initio classically, but existing attempts were not very successful. Our utility estimate will be valid either way, but it does not have to be quantum computers that succeed in this material search. A table of possible applications of MIT can be found in the supplement of [7], including:

- Memory
- Logic
- · Artificial Synapse
- · Artificial Neuron
- · Photodetector
- Gas Sensor

While most research focuses on making a transistor out of MIT material, it is not expected that it would replace conventional semiconductor technology for integrated circuits. Indeed, in the reviews discussing continuing Moore's law, MIT materials are not listed as a potential candidate for a new

transistor for conventional computers. There is a field, however, where it is considered promising: the field of neuromorphic computing. Indeed, the reviews [8] would list it as the 3rd best out of 6 potential candidate technologies, giving the weight factor of 1/5. There is no direct estimate for the market size of neuromorphic computing, but we could use AI market share of semiconducting hardware listed in [9] as 20%. The US semiconductor market is \$80b, while the global one is \$600b. We do not expect that the chip production using a completely new paradigm of neuromorphic computing can easily be reverse-engineered over a 10-year timescale, assuming that the details of the fabrication process are kept private early on, which means we can use the global revenue for our estimate. As the main financial investment in semiconductor manufacturing is the expensive fabrication facilities, not the research into the transistor technology itself, we estimate a 1/10 ratio of how the chip technology will factor in the revenue. Finally, we need to estimate the probability of switching from the current dedicated AI hardware to neuromorphic computing. Again, since there are various competing technologies (GPU, TPU, etc.), we estimate another 1/10 ratio as the neuromorphic devices take the last place out of 4 candidates. The resulting utility estimate is:

Utility =
$$\frac{1}{5} \times \frac{1}{5} \times \frac{1}{10} \times \frac{1}{10} \times \$600b = \$24M$$
 (3)

The size of the research grants spent on this search so far can be estimated from the reports on DOE programs and European collaborations. Q-MEEN-C in San Diego has been funded for eight years with \$3M per year, focusing on MIT materials and spintronics for neuromorphic computing. It also contains experimental effort in fabricating device prototypes. We expect roughly 1/10 of funding to go to the computational efforts, resulting in a \$2.4M scientific funding estimate of utility. We also note the Materials Project, from which we learn that about 100 materials with MIT are known [10], though the funding structure of that project does not allow an easy estimate, and 1.5M euro FIRSTORM program as an example of a smaller scale computational research program on this topic. It is clear that many other computational research programs on this topic were funded, raising the total scientific funding utility to 10x the amount we found (an order of magnitude estimate), \$20M. We note that the two estimates have produced a comparable number.

E. Gibbs state preparation: most likely targets

In this section, we discuss a subroutine of many quantum algorithms: using a thermal state as an initial state. Applications that allow for those initial states are the material searches such as the high-Tc and MIT material searches, as well as quantum chemistry problems that involve modeling materials such as surface chemistry. Some problems in fundamental science also require thermal initial states, such as the MagLab experiment on $\rm Ca_3Co_2O_6$ described above. We estimate the total utility of all the applications where Gibbs state prep is a reliable tool to be of the order of \$100M and refer to companion

publications for specific resource and utility estimates. While Gibbs state prep alone does not solve those applications, and each individual task in those \$100M can be only \$2M or less, with varying required number of runs, it may well be possible that Gibbs state preparation will dominate the resource cost. The reasons why one would still choose Gibbs state preparation instead of other approaches are explained below.

We first digress to discuss a more common problem of ground state preparation. To obtain the desired precision, existing algorithms of ground state preparation usually contain an unknown factor in the dependence of the total resource cost on the system size. For example, a ground state estimation algorithm can enhance the probability of the ground state for an initial state with nonzero overlap, with circuit size growing with the inverse overlap. The initial state is then constructed by another circuit, and the cost of that circuit is impossible to compute before the quantum computer actually becomes available. It is sometimes assumed that this circuit's cost is negligible, so only the ground state estimation resource cost is counted in the resource estimate. It is, in general, not known what is the class of Hamiltonians where a polynomial accuracy can be obtained in polynomial time. 1D matrix product states (MPS) of gapped Hamiltonians are one example of such a system [11]: it is proven that the MPS can be computed classically and then constructed as a circuit inside the quantum computer. The overheads of such a construction may be quite big, though. Besides the rigorously proven results, we also have intuition about the behavior of the quantum annealing approach to the preparation of the polynomial overlap state. Essentially, a path avoiding first-order phase transitions needs to be found connecting the target state to some accessible initial state, such as the lower overlap state prepared by other methods or the product state. First-order phase transitions, however, are quite common. Thus, the adiabatic state preparation cannot be applied blindly. Every target system's phase diagram needs to be analyzed independently. We see that there is no unified method for providing a resource estimate for the state preparation of application-relevant states. The best one can hope for is an extrapolation for small system sizes, where both positive and negative results have been claimed [12] since the accuracy of the extrapolation is not controlled by anything.

In comparison, thermal state preparation allows for more accessible guarantees. Indeed, the thermal state of any system can be prepared for sufficiently high temperatures [13]. Moreover, a bound exists [14] for the time to prepare the thermal state for all systems satisfying the Eigenstate Thermalization Hypothesis (ETH). Extrapolating the parameters in that bound from the exact diagonalization results would be more stable than extrapolating the overlaps in ground state estimation since those parameters reflect physical phenomena. The distinction between ETH and non-ETH systems is also well understood, with the latter containing many-body localization, spin glasses, and integrable models. Most of the application models are not in any of those categories. For example, glassy effects have never been observed in nonequilibrium electron dynamics of large molecules in quantum chemistry. That suggests that we could reliably prepare finite temperature states in

those systems by a universal algorithm. Compare it with the adiabatic ground state preparation, which relied on avoiding first-order phase transitions above. To the best of our knowledge, this is the only reliable way to obtain resource counts for the initial state preparation algorithms.

III. PROBLEM STATEMENT

In both application instances, we will formulate an open system evolution given by the master equation:

$$\frac{d\rho}{dt} = \mathcal{L}\rho := -i[H, \rho] + \sum_{\mu=1}^{M} (2L_{\mu}\rho L_{\mu}^{\dagger} - \{L_{\mu}^{\dagger}L_{\mu}, \rho\}) \quad (4)$$

by specifying the Hamiltonian H, initial state $\rho(0)$ and the Lindblad generators L_{μ} . While in our application instances, we will use simple local forms of L_{μ} , a variation of the same application instances that has a correct thermal steady state [15] and is more likely to produce valuable results uses $L_{\mu}^{\rm therm}$ defined via Hamiltonian evolution e^{iHt} of a simple local operator. Such an operator would generally span the entire system and contain exponentially many Pauli's, yet it can be evaluated efficiently on a quantum computer [15]. It is this operator that is used in our third, broad-scope application instance of preparing Gibbs states, which we do not discuss further as it directly follows [15].

A. MagLab's application problem (Ca₃Co₂O₆)

Quantum-Classical separation can be argued for from the results of [3]. In particular, in Fig. 7, the results of QMC are shown as a proxy for nonequilibrium open system dynamics. Our goal is to reproduce it. The corresponding experiment is shown in Fig. 1.

We note that while many MagLab studies correspond to closed system processes, the specific experiment shown in Fig. 1 is a **nonequilibrium open system evolution**. The model is a version of the Transverse Field Ising model. The longitudinal and transverse magnetic fields are controlled by the experimentalist. The spins are arranged in the following three sublattices as shown in Fig. 2.

 $J_1=-1$ is ferromagnetic, while $J_2=0.1|J_1|$ and $J_3=0.1|J_1|$ are antiferromagnetic. The overall energy scale is $23.9(2){\rm K}$, which can be translated into $4.98\cdot 10^{11}{\rm Hz}$. The z-component of the Hamiltonian is given by:

$$H_z(t) = \sum_{\gamma=1,2,3} J_{\gamma} \sum_{(i,j)_{\gamma}} \sigma_i^z \sigma_j^z - h(t) \sum_i \sigma_i^z$$
 (5)

An additional term is the transverse field $H_x = h_{TF} \sum_i \sigma_i^x$ with $h_{TF} = |J_1|/300$. The total Hamiltonian is $H(t) = H_z(t) + H_x$. The problem is to simulate the nonequilibrium states arising during the hysteresis loop: a sweep of the longitudinal field h(t). The longitudinal field h(t) is swept from 0 to $1.4|J_1|$ over a week of real time, $T = 5.57 \cdot 10^5 \mathrm{s}$

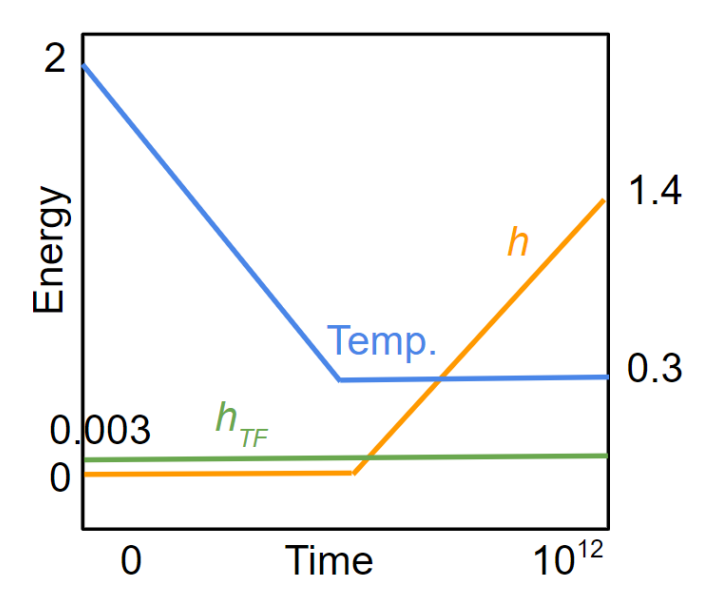


FIG. 1. The schedules used for a quantum simulation of an experiment [3] shortened from 1 week to 1s, in energy units $|J_1|=1$ and inverse energy units for time

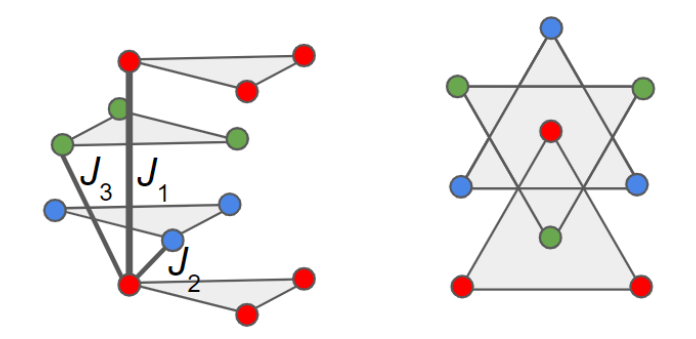


FIG. 2. Illustration of the layout of spins in $\text{Ca}_3\text{Co}_2\text{O}_6$. There are three alternating layers, each containing a triangular lattice of spins. The interactions are between layers, as shown. Four layers are shown on the left, and the view from the top is on the right.

 $=2.77\cdot 10^{17}$ in the units where $|J_1|=1$ in the original experiment. We will only consider T=1s= $4.97\cdot 10^{11}$ in natural units as it will turn out to be enough to illustrate how long nonequilibrium dynamics is still out of reach of quantum simulation. The schedule of sweeps is shown in the figure above.

An open question is how large does a transversal field need to be ($h_{TF} \sim |J_1|$ or 2000T is a conjecture) to remove the signatures of those nonequilibrium states - those fields cannot be probed in an experiment, and quantum simulation is the only tool that can access them.

The nonequilibrium values of the z-magnetization arise as the result of imperfect thermal relaxation. The only classical method that reproduces them is quantum Monte Carlo, which theoretically shouldn't have predictive power for nonequilibrium dynamics. Sometimes, it still works, but it cannot by itself be conclusive. A quantum simulator is the only tool that would potentially lessen MagLab's workload and also answer the question it cannot access.

Here, we specify the open system addition to the above Hamiltonian that would reproduce the data as shown. The simplest way that may already describe the data is to add Lindblad operators $\sim \sigma^- = |0\rangle\langle 1|$ and $\sigma^+ = |1\rangle\langle 0|$ conditioned on the states of neighboring spins, with rates given by the classical energies of the computational basis spin configurations.

$$L_{i,r_{\pm},\pm} = r_{\pm} P_{r_{\pm}} \sigma_i^{\pm}, \qquad (6)$$

$$P_{r_{\pm}} = \sum_{s:r_{\pm,s}=r_{\pm}} \left(\prod_{j \in NN(i)} P_{j,s_j} \right) \tag{7}$$

$$r_{\pm} \in \{r_{\pm,s}\}, \quad r_{+,s} = \text{MC rates for } H_z =$$
 (8)

$$= \begin{cases} e^{-\beta \Delta E}, & \text{if } \Delta E > 0\\ 1, & \text{otherwise} \end{cases}$$
 (9)

where
$$\Delta E = H_z^{(i)}(s, +1) - H_z^{(i)}(s, -1)$$
, (10)

and $P_{j,s_j}=\frac{1}{2}(\sigma_j^z+s_j)$ is a projector onto a state $|s_j\rangle$. The energies $H_z^{(i)}(s,s_0)$ are the terms of H_z containing σ_i^z , after the substitution $\sigma_j^z\to s_j$ for all neighbors $j\in NN(i)$ in the interaction graph, and $\sigma_i^z\to s_0$. The inverse temperature β is taken from the schedule in Fig. 1. Here we joined the spin flips for particular configurations of the neighbors that happen to have equal rate into a single L_μ operator, so that it would preserve the coherence between different states of the neighbors in that case. $P_{r\pm}$ are the corresponding joined projectors that may have rank higher than 1. r_+ and r_- iterate through all possible values of the rates $r_{\pm,s}$. We note that $r_\pm=1$ is the most frequent as well as the highest rate, with about a half of all configurations. The number of terms $L_{i,1,+}$ and $L_{i,1,-}$ is the range of index i, which is the total number of spins.

Due to a very small value of h_{TF} , this choice of L_{μ} may be sufficient to reproduce the nonequilibrium plateau observed in the experiment, and either positive or negative result will shed light on the underlying physics of the phenomenon. A more advanced approach that is more likely to reproduce the experiment is using L_{μ}^{therm} as defined in [15].

The smallest size expected to show relevant physics is 25 layers of 9×9 lattices (2,025 spins). As the three plateaus that are seen in the nonequilibrium magnetization are steps of about 10% of the full magnetization range, we set the required error in the measurement of total magnetization to 10%.

For the simulation time, the week of the actual experiment can be accelerated by increasing the bath coupling. Let us assume that a 100-fold increase is possible. We will further simplify the task, requiring that the simulation needs to model just $T=1\mathrm{s}$ duration of the experiment. The precise sweep of the magnetic field is not necessary, so we just need to increase it in steps for 10 steps to observe the same behavior. The precision of each step is 0.01.

B. Metal-Insulator transition material search application problem

We will now specify an application instance corresponding to the entire material search in the MIT space. We estimate that the search will need to cover 1000 models of materials at 1000 parameter points each. Indeed, currently, ~ 100 materials with MIT are known [10], and we take one order of magnitude higher number as the size of the search space. One thousand parameter points will contain 10 values of temperature, doping, and orbitals kept in the downfolding of the ab initio model.

We suggest starting the search with t-J model transport on a 10×10 grid, which we will use in the Landauer setup [16] (attaching fermion sources and sinks on the left and right edge) as the foundation for the resource estimate. 4×4 grid has been done classically via exact diagonalization and Kubo formula[17], while 10x10 is large enough to be classically challenging and make the finite size effects negligible. A simulation of transport in an integrable model shows the non-universal effect of sources and sinks to extend only 2-3 sites in [18, Fig. 5].

We expect that the material search will start with simple problems like the 10×10 example and eventually go into the ab initio investigation as guided by the experts analyzing the results of the previous runs. Such an investigation may require up to 300 orbitals per site. We will use the average 150 orbitals for the resource estimate between the low-end and high-end costs. 300 orbitals per site were used in [5] for ab initio prediction of superconducting order (which then was used to roughly predict T_c).

Our application instance is a direct generalization of the problem considered [17]. It is a t-J model on a square lattice:

$$H = -\sum_{i,j,s} t_{ij} \tilde{c}_{js}^{\dagger} \tilde{c}_{is} + J \sum_{\langle ij \rangle} (\mathbf{S}_i \mathbf{S}_j - \frac{1}{4} n_i n_j)$$
 (11)

Each lattice site contains two fermionic modes labeled by $s=\pm 1.$ The $\tilde{c}_{i,s}^{\dagger}=(1-n_{i,-s})c_{i,s}^{\dagger}$ are projected creation operators that do not allow the creation of the double-occupancy states, thus satisfying the Hubbard term $Un_{i,s}n_{i,-s}$ perfectly, which is why it is not present in Eq. (11). The perturbative interaction $J=2t^2/U$. Here $n_{i,s}=\sum_s c_{i,s}^{\dagger}c_{i,s}$ and $S_i^\mu=\frac{1}{2}\sum_{ss'}c_{i,s}^\dagger\sigma_{ss'}^\mu c_{i,s'}$, where σ^μ are Pauli matrices. The hoppings contain nearest-neighbor and next-nearest neighbor terms t and t' = -0.15t. The exchange J = 0.3t and [17] take t = 0.3eV. These choices are typical for downfolded models of cuprates. The t-J model is an approximation to the Hubbard model, obtained from the corresponding Hubbard Hamiltonian perturbatively and by restricting to zero and single occupancy subspace of the Hilbert space. In other words, states with two fermions of opposite spin on at least one of the sites are not included in the Hilbert space. The projections are appropriately included in the definition of the creation annihilation operators in the Hamiltonian above. On a quantum computer, we will model the full Hilbert space anyway, so one could instead simulate a simpler Hubbard model. We leave the t-J model in this application study for the direct comparison with [17]. We expect that the finite-size effects will not be as prominent at larger system sizes; therefore, we will use open boundary conditions. The authors compute conductivity

via the Kubo formula as a function of frequency ω , averaged over various boundary conditions, and apply broadening by $\epsilon=0.07t$. This broadens the delta functions present due to coherent no-scattering transport. After that broadening, they evaluate the resistivity as $6.6\mathrm{A}/(\mathrm{conductivity}(\omega=0)e_0^2/\hbar)$ and find good agreement with experimental values.

The initial state of the model above is characterized by a parameter c_h describing the number of holes in the system, which is a conserved quantity of the Hamiltonian. For example, $c_h = 3/20$ means that the system of 20 sites is doped in such a way that three positions are unoccupied, and all the other positions are occupied by 1 electron each. As the initial states are not required to be in equilibrium, any fermionic state with this fraction of excitations can serve as an initial state. For example, one may start with each position singleoccupied, and then destroy electrons on the first $c_h L^2$ sites for an $L \times L$ lattice. To formulate an open system problem equivalent to the Kubo formula used in [17], we set up sources and sinks for the electrons on two opposite sides of the square lattice, thus breaking the conservation. To derive the Lindblad operators for sources and sinks, one needs to specify the spectral density $\gamma_{L,R}(\omega)$ of the creation-annihilation operators in our system as a function of temperature and chemical potential. This may be done either as a separate task on a quantum computer or classically using a smaller size patch or a free fermion approximation of the system to compute correlation functions and spectral density. Either way, an efficiently computable interpolation for the spectral density needs to be used. One then would use the obtained spectral density to build the Lindblad operators L_{μ}^{therm} on the left and right boundary from the hopping terms split by the system boundary, with spectral densities for two different values of chemical potential on the left and the right side, according to the general prescription of

For our resource estimate, we will use the simplest possible case $L_{\text{left}} = c$ and $L_{\text{right}} = c^{\dagger}$ on every site of the left and right edges of the square lattice, as it corresponds to some high temperature. If this system equilibrates for a time T, the transport obtained would be roughly equivalent to the broadening of the delta functions in the closed system Kubo formalism used in [17] by 1/T. The local temperature and chemical potential can be measured by fitting an observable, such as the local part of H, or the density n, to a small system size values in a Gibbs state obtained via exact diagonalization. The electric field E can be found as the gradient of the chemical potential. Finally, one measures the current operator j (one boundary part of [H, n] where n is the density in some region of the system). According to Maxwell's equations, the conductivity = j/E. In other words, the task for the quantum simulation is to measure n and a group of local terms of H in some portion of the system enough to estimate the gradient of the underlying chemical potential, as well as the current j. All of these measurements can be performed in a single shot since the system is much larger than the 4×4 size accessible classically. The non-commuting terms in the Hamiltonian can be measured at various locations perpendicular to the current direction. The temperature can be taken as the system average. After that, one point can be placed on the plot of resistivity

= 1/conductivity. To compare with the 4x4 results of [17], one may need to convert it to physical units using the lattice spacing of 1.65A and the quantum of conductance.

Classical state-of-the-art Recent ab initio numerical investigation by [5] shows that even the high-Tc transition temperature can now be predicted by numerical techniques. Since the metal-insulator transition in application-relevant materials happens at higher temperatures, there is a possibility that classical techniques may predict it fully ab initio as well. The apparent absence of publications on this topic may be due to conceptual difficulties with computing a transport coefficient numerically from first principles (unknown disorder, different assumptions of Kubo and Landauer approaches, apparent divergence of DC conductivity without disorder), not due to computational hardness. We also note that machine learning may be successful in the material search for MIT materials, with some initial results presented in [10]. Finally, the cost of searching for MIT transitions experimentally at room temperatures may not be very high for cheap fabrication methods. What makes large throughput experimental material searches unfeasible in condensed matter is that the material properties are highly sensitive to fabrication quality, and such a search would also require automated optimization of fabrication technology for each material. Another concern is that many of the candidate materials are toxic.

IV. QUANTUM IMPLEMENTATION

Many algorithms for tasks related to ours have been proposed. Below we list the promising alternative approaches before describing the approach we believe to be optimal:

- Thermal Sampling [19] we found the resource cost estimate of this algorithm hard to apply to the systems we consider.
- Thermalizing Open Systems with exact fermionic baths [14]. While it does not implement every Lindbladian, it covers the ones we need for both of our application instances. We believe that the algorithmic cost of these baths has suboptimal scaling.
- Kraus operators corresponding to the Lindblad evolution for a short time can be used together with various quantum algorithms to implement quantum channels given Kraus operators. For example, [20] were able to realize a circuit compact enough for NISQ devices. That approach appears to have highly unfavorable scaling with the evolution time.

What we are interested in is commonly referred to as quantum signal processing (QSP) scaling, which refers to $T\log(1/\epsilon)$ scaling of the algorithm runtime with evolution time T and precision ϵ , possibly at the cost of extra powers of the system size in front.

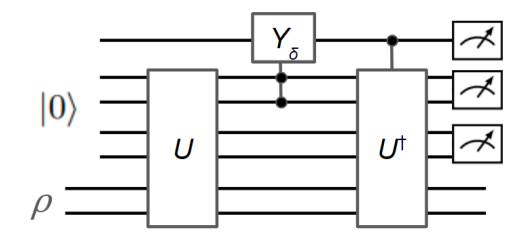


FIG. 3. A simple circuit approximately implementing an open system evolution $e^{\delta \mathcal{L}} \rho$ via the block-encoding of a Lindbladian U. The gate $Y_{\delta} = e^{-iY \arcsin \sqrt{\delta}}$

A. Lindbladian OSP

We will follow the approach of [15] to achieve QSP scaling for a Lindbladian. First, consider a simple (not achieving QSP scaling) evolution step in the language of [15] via the circuit in Fig. 3.

Here U is a block encoding of a Lindbladian, containing all the Lindblad operators conditioned on the value of the ancilla. Iterating this is the simplest way to simulate the open system dynamics. A more advanced algorithm also found in [15] achieves QSP scaling for the number of gates. Specifically, Theorem III.2 of [15] uses a circuit more advanced than shown above, a compression algorithm on the number of applications of the Lindbladian in the weak measurement version of QSP. To our knowledge, there are no QSP scaling algorithms for time-dependent Lindbladians. Developing them is an important direction for future work. The only QSP scaling algorithm for closed system time-dependent Hamiltonian is [21].

V. RESOURCE ESTIMATION FOR PROPOSED QUANTUM ALGORITHMS

While Lindbladian QSP may have an optimal scaling (except for the factor of the system size due to block encoding), for smaller system sizes, other algorithms, such as exact fermionic baths, may have an advantage in gate count. As the gate count for both is only available in terms of big-O notation, these algorithms require new resource estimates.

We note that to do the resource estimates for the applications, we need to specify the time to run the algorithm. For the preparation of the equilibrium state, this time is a property of the Lindbladian. In principle, it can be extrapolated from the sizes that can be addressed classically. If those sizes prove too small, one can use the formula in [14] relating the relaxation time to the parameters of the eigenstate thermalization hypothesis, which may be determined at smaller sizes.

For $Ca_3Co_2O_6$ and MIT material applications, we do not actually need to prepare the Gibbs state accurately. The nonequilibrium states seen before the system fully relaxes are the target for quantum simulation of $Ca_3Co_2O_6$, so the simulation time should match the experiment duration, or at least 1s of it as the minimum we set. For MIT materials, one approach is to rescale the time corresponding to the broadening

0.07t used in [17] by a factor of $150 \cdot 10/4 = 375$ due to the increase in the linear size of the system (L=10) and the average number of orbitals (150). In other words, T=375/0.07t.

We note that [17] computed the resistivity using the Kubo formula, which would translate into a closed system algorithm that measures the Fourier transform of the correlation function and subsequently integrates it. It may be possible to obtain a comparable performance of this algorithm by performing all the integration inside the quantum algorithm, but naively the open system algorithm requires doing the dynamics just once to obtain the steady state and measure the flow directly, while the closed system algorithm requires performing the dynamics multiple times and integrating the results. We will only do the resource estimate for the open system case.

Below, we provide the order of magnitude resource estimates.

A. Abstract Logical

1. Lindbladian QSP

Theorem III.2 of [15] lists the following requirements for simulating the open system time evolution for time t to precision ϵ . It relies on the block encoding of the Lindbladian \mathcal{L} governing the evolution, i.e. a unitary U such that all M Lindblad generators L_{μ} can be found as blocks in the upper left corner of it:

$$U = \begin{pmatrix} L_1 & L_2 & \dots & L_M & \cdot \\ \vdots & \vdots & \ddots & \vdots & \cdot \end{pmatrix}$$
 (12)

Let c be the number of ancillas used by the block encoding of Lindbladian U. The quantum algorithm uses $O((c+\log((t+1)/\epsilon))\log((t+1)/\epsilon))$ resettable ancillas, $O((t+1)\log((t+1)/\epsilon)/\log\log((t+1)/\epsilon))$ controlled uses of U and its conjugate, same amount of uses of V that block encodes the Hamiltonian, and $O((t+1)(c+1)\operatorname{polylog}((t+1)/\epsilon))$ other 2-qubit gates.

2. Block encoding for a Lindbladian

The block encoding used for efficiently implementing $L_{\mu}^{\rm therm}$ used for Gibbs state preparation is developed in [15]. Those generators rely on the ability to implement the controlled closed system evolution, as well as the custom gates $Prepare, V_{jump}$ that, together with quantum Fourier transform (QFT) allow to integrate that closed system evolution. We do not go into the detail of that construction, providing a high-level overview of the circuit in Fig. 4.

The total cost is given in Lemma I.1 of [15]: the maximum closed system controlled simulation time is T_{CG} , the internal parameter of $L_{\mu}^{\rm therm}$, and besides n system qubits extra ancillas logarithmic in the number of jump operators A and in the Fourier discretization grid size N are used. The internal simulation time T_{CG} and grid size N are specified in [15]. We note that for preparing the equilibrium state (in contrast to the

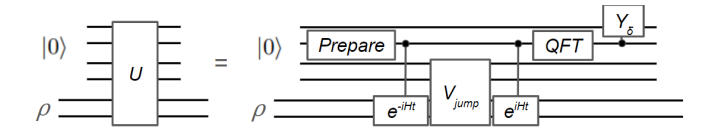


FIG. 4. A circuit for the block-encoding of a thermal Lindbladian U used in [15]. The gate $Y_\delta=e^{-iY \arcsin \sqrt{\delta}}$ and here $\delta=1-\gamma(\omega)$ is taken conditionally on the frequency of each contribution to the Lindblad operator

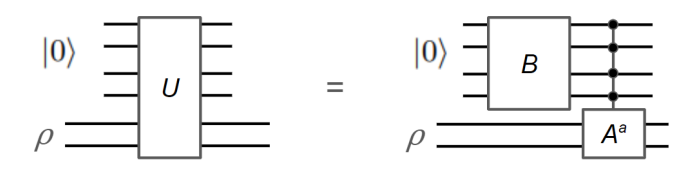


FIG. 5. A circuit for the block-encoding of a Lindbladian ${\cal U}$ given by its unitary Lindblad generators.

open system evolution), this is not the optimal algorithm, and the authors of [15] present further refinements.

For our application instances with simpler Lindbladians, we use the internal structure of V_{jump} in [15]. A set of unitary operators A^a is block encoded in it as follows:

$$V_{jump} = \left(\sum_{a \in A} |a\rangle\langle a| \otimes A^a\right) \cdot (B \otimes I_{\text{sys}}), \quad (13)$$

where the operator B prepares a uniform superposition $B|0\rangle=\sum_{a\in A}\frac{1}{\sqrt{|A|}}|a\rangle$ following [22]. For the simplest case where $L_a=A^a$ which are unitary, the block encoding of the Lindbladian is just $U=V_{jump}$ illustrated in Fig. 5. Since in our case the operators L_μ are not unitary, and have O(1) cases of different coefficients in front, we will need to utilize an O(1) number of extra ancillae for the block encoding.

For $\text{Ca}_3\text{Co}_2\text{O}_6$, the Lindblad terms (Eq. (6)) contain σ^\pm multiplied by projectors onto the state of a constant number of neighboring spins. For MIT problem, after the Bravyi-Kitaev transformation [23] from fermions to qubits the creation-annihilation operators would have a logarithmic weight, containing a product of Pauli's and one σ^\pm . We will now briefly outline a possible (not necessarily optimal) block-encoding, and show that the added complexity is subleading anyways. First we note that σ^\pm and can be block encoded into a 2-qubit permutation:

$$\left(\begin{array}{c|c}
\sigma^{-} & \cdot \\
\hline
\cdot & \cdot
\end{array}\right) = \left(\begin{array}{c|c}
0 & 0 & 1 & 0 \\
1 & 0 & 0 & 0 \\
\hline
0 & 1 & 0 & 0 \\
0 & 0 & 0 & 1
\end{array}\right), \quad \left(\begin{array}{c|c}
\sigma^{+} & \cdot \\
\hline
\cdot & \cdot
\end{array}\right) = \left(\begin{array}{c|c}
0 & 1 & 0 & 0 \\
0 & 0 & 1 & 0 \\
\hline
1 & 0 & 0 & 0 \\
0 & 0 & 0 & 1
\end{array}\right) \tag{14}$$

A conditioned product $C(U_1 \otimes U_2)$ of 2 unitaries U_1, U_2 acting on two different sets of qubits can be implemented as a sequence of CU_1 and CU_2 , which allows to implement the block encoding of creation-annihilation operators.

A k-qubit rank-1 projector can be encoded using a 2k-qubit permutation:

$$\begin{pmatrix}
1 & 0 & \dots & 0 & 0 & 0 & 0 & \dots & 0 & 0 \\
0 & 0 & \dots & 0 & 0 & 1 & 0 & \dots & 0 & 0 \\
0 & 0 & \dots & 0 & 0 & 0 & 1 & \dots & 0 & 0 \\
\dots & \dots \\
\hline
0 & 0 & \dots & 0 & 0 & 0 & 0 & \dots & 1 & 0 \\
\hline
0 & 1 & \dots & 0 & 0 & 0 & 0 & \dots & 0 & 0 \\
\dots & \dots \\
0 & 0 & \dots & 0 & 1 & 0 & 0 & \dots & 0 & 0 \\
0 & 0 & \dots & 0 & 0 & 0 & 0 & \dots & 0 & 1
\end{pmatrix}$$
(15)

Since k=O(1), only a constant number of ancillae is required for the implementation of the MC spin flip rate operators.

Finally, if there are m = O(1) distinct rates in front of M Lindblad terms, we may use additional $\log m$ ancillae, prepare a state of it where the amplitudes reflect the desired rates, and then condition $B_S(B_S|0) = \sum_{a \in S} \frac{1}{\sqrt{|S|}} |a\rangle$ for each subset S of A with the same rate on the state of these ancillae. For MIT material, all M terms have the strength $1/\sqrt{M}$, which effectively requires the increase in the evolution time by a factor of $\alpha = M$. For Ca₃Co₂O₆, the terms that lower the energy have the maximal rate 1. There is one such term for each spin. We will assume that those terms dominate the amplitude, thus time will effectively increase by a factor $\alpha = 2025$, the system size. The total number of terms M is at most $2025 \cdot 2^d$, where d is the degree of the interaction graph. A more careful estimate of possible neighbors goes as follows. From Fig. 2 we see that there are 2 neighbors linked by J_1 and 12 neighbors linked by $J_2 = J_3$. There are m+1 possible values of the total spin for m spins. Thus the number of possible rates is $3 \cdot 13$ (we took into account that half of them lower the energy and thus map to 1). We will use $M \sim 39 \cdot 2025$ the Ca₃Co₂O₆ instance.

The block encoding of L_{μ} for all $\mu=1\dots M$ only involves the register of $c\sim \log_2 M+O(1)$ size that is used to control individual L_{μ} . The number of ancillae used by the logical algorithm utilizing this block encoding and Lindbladian QSP is $O((\log M + \log((t+1)/\epsilon))\log((t+1)/\epsilon))$, which is subleading compared to the system size.

B. Compiled Logical

The weight of Bravyi-Kitaev [23] creation operator goes logarithmic with the system size 10×10 in the MIT example, but we will treat it as a small constant. In other words, we will assume that each L_{μ} is local in what follows.

As we have seen in the previous section, U involves the select step $|\mu\rangle\langle\mu|\otimes L_{\mu}$ with M gates, each of which is $\log_2 M$ -controlled application of L_{μ} . The T-gate count of an individual such gate would be $\sim 4\log_2 M$, T-depth $\sim 4\log_2\log_2 M$ and depth $\sim 16\log_2\log_2 M$ [24], and the gates are applied in sequence. At the expense of increasing the number of ancillae to M, it would be possible to instead use one-hot encoding

for ancillae and single controlled gates for $|\mu\rangle\langle\mu|\otimes L_{\mu}$ in constant depth, as many of the operators L_{μ} act on independent sets of qubits and may be parallelized. The *Prepare* step B for such a one-hot encoding, however, would still require $\sim M$ depth and T-cost. These ideas are further refined in [25], yet we do not apply those results here. Instead, we estimate the leading contribution to the cost of U of the best method to be: $\sim 10 M \log M T$ -gates, $10 M \log \log M depth$, where $\log M \log M depth$ is now the same as \ln base e. The number of ancillae still scales as $c \sim \log_2 M$. The algorithm for QSP evolution using U also uses other gates. We will also assume that the 2-qubit gate count $\sim t \log M \log t/\epsilon$ from the QSP can be roughly interpreted as the T-gate count, as it is subleading anyways.

The size $M=2\cdot 10\cdot 150$ for the MIT material application (two boundaries of L=10 sites each with 150 orbitals on average throughout our material search, and the fermion is created or annihilated in each orbital), and $M = 39 \cdot 2025$ for the Ca₃Co₂O₆ (thermalizing every spin). This results in the T-cost of block encoding U as $10M\log M = 240,000$ and 150, 000, respectively. The depths are 60, 000 and 40, 000 respectively.

Recall that the algorithm in Theorem III.2 of [15] uses the following number of consecutive calls to the block encoding

$$O\left((\alpha t + 1) \frac{\log((\alpha t + 1)/\epsilon)}{\log\log((\alpha t + 1)/\epsilon)}\right)$$
 (16)

where α is the time upscaling factor discussed above (α = 3000 and 2000 for the two cases we consider). To estimate the T-gate count, we multiply it by the cost of the block encoding (we neglect the increase in T-count due to the controlled use of U), and drop the constabt factor hidden in the big-O notation:

$$#T = \alpha t \frac{\log(\alpha t/\epsilon)}{\log\log(\alpha t/\epsilon)} 10M \log M , \qquad (17)$$

and same with loglog M for the depth. For the MIT material application t = 54000 and $\epsilon = 0.1$, while for Ca₃Co₂O₆, we need to makes 10 steps of $t = 10^{11}$, each with precision $\epsilon = 0.01$. Plugging in these numbers, we get:

	MIT search	
T-count	$2.7 \cdot 10^{14}$	$1.9 \cdot 10^{23}$
T-depth	$7.0 \cdot 10^{13}$	$4.0 \cdot 10^{22}$

We see that the parallelism in T-gate application is not substantial in this estimate, accounting for only $\times 1/4$ reduction in runtime compared to applying T-gates one at a time. In other words, the algorithm consumes 4 T gates per gate layer on average. Ideally, $\times 1$ /number of qubits reduction should be possible, yet the OSP algorithms we use do not allow it. We also note that for the MIT material application, the Hamiltonian part of the evolution (not estimated here) may, in fact, be the leading contribution.

C. Physical

To estimate the physical requirements, we follow the resource estimate in [26, Table IV]. The T-count can be found in the column M, and $(ns, 10^{-3})$ is the closest relevant noise parameter for superconducting technology in that reference. We first see that the runtime is roughly 10^{-6} s times the Tcount across the application instances they consider.

We multiply the T-gate counts by 10^{-6} s to estimate the total runtime. Since Ca₃Co₂O₆ only needs to be executed once, that results in $1.9 \cdot 10^{17}$ seconds (6 · 10⁹ yrs), an unrealistic number. Each run of MIT material search requires only $2.7 \cdot 10^8$ s (8.6 years). We will be able to reduce that number at the cost of increasing the number of qubits below.

A more careful resource estimate for the physical count would proceed as follows. We will follow a recent short paper [27]. Specifically, we note that Fig. 17 in it allows one to draw a line through the qubitcycle resource estimate between 10^{-4} and 10^{-10} error rate of the T-state: we get 100,000 qubitcycles per each power of 10 below 10^{-4} individual T-state error. Table II of [27] allows us to estimate the time and space requirements: the rightmost cluster of star symbols have 78 cycles and 10614 qubits, which gives the ratio of the two in the qubitcycle number. The required error of the distilled state is roughly the target error ϵ /number of T gates. The time of the code cycle is 4 CNOTs and a measurement. In [26], we find the cycle time from Table II to be 300ns. The resulting costs per factory become:

Factory time cost = $13(|\log_{10}(\epsilon/\#T)| - 4)$ cycles = $0.4(|\log_{10}(\epsilon/\#T)| - 4)\mu s$

Factory qubit cost= $1,800(|\log_{10}(\epsilon/\#T)|-4)$ We will extrapolate beyond 10^{10} T-gates, though the factory costs may not be the leading cost in that regime. For the two cases we consider, the numbers are:

MIT: 150 cycles, 21,000 qubits, $d \sim 40$

 $Ca_3Co_2O_6$: 280 cycles, 38,000 qubits, $d \sim 50$

The distances are just rough guesses and can be further refined using the surface code threshold formula if necessary. For the entire algorithm, a tradeoff between using multiple factories or using fewer qubits but taking longer is possible. With a single factory, we estimate the total number of physical qubits as the factory size plus d^2 times the logical number of qubits, and the runtime is

$$300 \text{ns} \times \#T\text{-gates} \times \text{Factory time cost in cycles}$$
 . (18)

The factor ends up $4.4 \cdot 10^{-5}$ s and $8.3 \cdot 10^{-5}$ s times the number of T-gates for our two applications.

With multiple factories, one of the limiting factors is the number of T-gates per layer. If the algorithm consumes on average k T-gates per layer (in our case k = 4), then generating more T-states than $k \times \text{Factory}$ time cost in cycles is not useful as they will just idle until their time in the algorithm comes. So the number of factories n_f can vary between 1 and $k \times \text{Factory time cost in cycles.}$ An additional consideration for this tradeoff is the routing time. We will assume the naive picture where there are pathways between factories, and the throughput of 1 T-state per cycle is possible for each path-

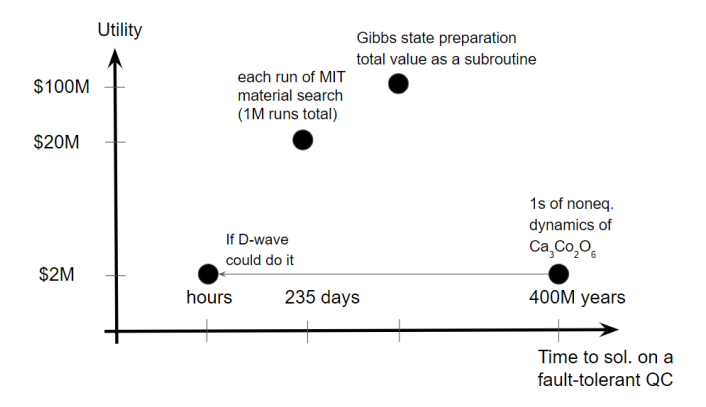


FIG. 6. We plot the three discussed applications of open system quantum simulation. It should be assumed that the points have 1-2 orders of magnitude error bars

way. A more careful consideration may restrict this further, thus restricting n_f . In the case of our two examples, we get:

	MIT search	Ca ₃ Co ₂ O ₆
total runtime (cycles)	$4 \cdot 10^{16}/n_f$	$5 \cdot 10^{25}/n_f$
total runtime (s)	$1.2 \cdot 10^{10}/n_f$	$1.5 \cdot 10^{19} / n_f$
#factory qubits	$21000n_f$	$38000n_f$
range of n_f	1600	11100
runtime (s) for max n_f	$2.0 \cdot 10^{7}$	$1.4 \cdot 10^{16}$
	(235 days)	$(4 \cdot 10^8 \text{ yrs})$

We see that for $n_f=44$ for MIT and $n_f=83$ for the ${\rm Ca_3Co_2O_6}$, the rule of thumb $10^{-6}{\rm s}$ per T-gate is satisfied. We also see that this time cost can be further reduced at the expense of a larger quantum computer. In particular, $6\cdot 10^9$ yrs are reduced to 3400 years on a 42 million qubit device for ${\rm Ca_3Co_2O_6}$ (here, the non-factory $\sim 5{\rm M}$ qubit cost is subleading). For MIT search, each run can now complete in 235 days using 12M factory qubits and $\sim 24{\rm M}$ non-factory qubits. We need to execute 10^3 runs for each model, which, if executed in parallel on multiple quantum computers, will give experts

time to come up with the next model. We expect only the hardest models, say 1% of 1000 suggested ones, to be sent to the quantum computer, while others investigated by classical methods or experimentally.

We collect the results of our estimates on the resource estimate vs. utility plot in Fig. 6. For completeness, we also indicate where analog quantum simulators[28] may lie. While the runtime of the universal quantum computer appears discouraging, we would like to note that our estimate is neither overly optimistic or overly pessimistic. The numbers may improve with the invention of a qubit hardware faster or more noise-resilient than the current superconducting qubit technology with 10^{-3} error rate and 300ns code cycle that we used. We also expect algorithmic improvements as the open system simulation algorithms are in early stages of development. The fault-tolerant architecture itself may change as the first experimental tests of it enable its optimization beyond the conventional T-state distillation approach. On the other hand, the factors in big-O notation and the subleading terms, as well as the contribution of the Hamiltonian dynamics we dropped in this estimate would likely increase our numbers by several orders of magnitude. The hardware may also experience new limitations as it is scaled up to tens of millions of qubits, which are unseen in the current generation of devices. We hope our investigation pointed out the urgent open questions in the field and provided a more tempered expectation for a broader community.

VI. ACKNOWLEDGMENTS

We thank Tameem Albash and Joshua Job for contributing to an early version of the draft. This material is based upon work supported by the Defense Advanced Research Projects Agency (DARPA) under Contract No. HR001122C0063. All material, except scientific articles or papers published in scientific journals, must, in addition to any notices or disclaimers by the Contractor, also contain the following disclaimer: Any opinions, findings and conclusions or recommendations expressed in this material are those of the author(s) and do not necessarily reflect the views of the Defense Advanced Research Projects Agency (DARPA).

^[1] R. Cleve and C. Wang, arXiv preprint arXiv:1612.09512 (2016).

^[2] National Research Council and Division on Engineering and Physical Sciences and Board on Physics and Committee to Assess the Current Status and Future Direction of High Magnetic Field Science in the United States (2013).

^[3] I. Nekrashevich, X. Ding, F. Balakirev, H. T. Yi, S.-W. Cheong, L. Civale, Y. Kamiya, and V. S. Zapf, Physical Review B 105, 024426 (2022).

^[4] A. Jain, S. P. Ong, G. Hautier, W. Chen, W. D. Richards, S. Dacek, S. Cholia, D. Gunter, D. Skinner, G. Ceder, et al., APL materials 1 (2013).

^[5] Z.-H. Cui, J. Yang, J. Tölle, H.-Z. Ye, H. Zhai, R. Kim, X. Zhang, L. Lin, T. C. Berkelbach, and G. K. Chan, arXiv preprint arXiv:2306.16561 (2023).

^[6] T. Wei, Y.-H. Huang, R. Zeng, L.-X. Yuan, X.-L. Hu, W.-X. Zhang, L. Jiang, J.-Y. Yang, and Z.-L. Zhang, Scientific Reports 3, 1125 (2013).

^[7] Y. J. Lee, Y. Kim, H. Gim, K. Hong, and H. W. Jang, Advanced Materials 36, 2305353 (2024).

^[8] J. Tang, F. Yuan, X. Shen, Z. Wang, M. Rao, Y. He, Y. Sun, X. Li, W. Zhang, Y. Li, et al., Advanced Materials 31, 1902761 (2019).

^[9] G. Batra, Z. Jacobson, S. Madhav, A. Queirolo, and N. Santhanam, McKinsey and Company, January 2 (2019).

- [10] A. B. Georgescu, P. Ren, A. R. Toland, S. Zhang, K. D. Miller, D. W. Apley, E. A. Olivetti, N. Wagner, and J. M. Rondinelli, Chemistry of Materials 33, 5591 (2021).
- [11] A. M. Dalzell and F. G. Brandão, Quantum 3, 187 (2019).
- [12] S. Lee, J. Lee, H. Zhai, Y. Tong, A. M. Dalzell, A. Kumar, P. Helms, J. Gray, Z.-H. Cui, W. Liu, et al., Nature communications 14, 1952 (2023).
- [13] Á. M. Alhambra and J. I. Cirac, PRX Quantum 2, 040331 (2021).
- [14] C.-F. Chen and F. G. Brandão, arXiv preprint arXiv:2112.07646 (2021).
- [15] C.-F. Chen, M. J. Kastoryano, F. G. Brandão, and A. Gilyén, arXiv preprint arXiv:2303.18224 (2023).
- [16] R. Landauer, Zeitschrift für Physik B Condensed Matter 68, 217 (1987).
- [17] M.-M. Zemljič and P. Prelovšek, Physical Review B 72, 075108 (2005).
- [18] T. Prosen, New Journal of Physics 10, 043026 (2008).
- [19] T. S. Cubitt, arXiv preprint arXiv:2303.11962 (2023).
- [20] Z. Hu, K. Head-Marsden, D. A. Mazziotti, P. Narang, and S. Kais, Quantum 6, 726 (2022).
- [21] J. Haah, M. B. Hastings, R. Kothari, and G. H. Low, SIAM Journal on Computing 52, FOCS18 (2021).
- [22] A. Shukla and P. Vedula, Quantum Information Processing 23, 38 (2024).
- [23] S. B. Bravyi and A. Y. Kitaev, Annals of Physics 298, 210 (2002).
- [24] Y. He, M.-X. Luo, E. Zhang, H.-K. Wang, and X.-F. Wang, International Journal of Theoretical Physics **56**, 2350 (2017).
- [25] R. Babbush, C. Gidney, D. W. Berry, N. Wiebe, J. McClean, A. Paler, A. Fowler, and H. Neven, Physical Review X 8, 041015 (2018).
- [26] M. E. Beverland, P. Murali, M. Troyer, K. M. Svore, T. Hoefler, V. Kliuchnikov, G. H. Low, M. Soeken, A. Sundaram, and A. Vaschillo, arXiv preprint arXiv:2211.07629 (2022).
- [27] Y. Hirano, T. Itogawa, and K. Fujii, arXiv preprint arXiv:2404.09740 (2024).
- [28] A. D. King, C. D. Batista, J. Raymond, T. Lanting, I. Ozfidan, G. Poulin-Lamarre, H. Zhang, and M. H. Amin, PRX Quantum 2, 030317 (2021).
- [29] B. Pozsgay, arXiv preprint arXiv:2402.02984 (2024).
- [30] L. G. Gunderman, A. J. Jena, and L. Dellantonio, arXiv preprint arXiv:2308.01986 (2023).

Appendix A: Planted solution problems

To accompany our application instances where the answers are unknown, here we suggest some planted solution instances with known answers but no direct application relevance, including the open system and the closed system versions. In the latter, we note the possibility of obfuscation that would prevent discovering the underlying planted solution.

1. Closed system: Integrable models and T-gates

Some prior work on breaking the type of obfuscation considered below can be found in [29] and references therein. The theorems those references prove concerned themselves with the situation when the solution is known via some free fermion ansatz for any value of coefficients of the Hamiltonian

terms. Then, given just the terms, one can always recover the ansatz. In the construction below, the model is solvable only for fine-tuned values of coefficients, and these theorems are not applicable.

The problem is formulated as follows. Input:

- A superposition of stabilizer states defined on n qubits.
 Instead of specifying the state, the operators (in our case, Pauli operators) that stabilize the state are provided.
- A Hamiltonian on n qubits expressed as a linear combination of Pauli operators.
- A total simulation time T.
- List of observable(s) A.
- Desired relative error ϵ .

Output:

• Expectation value of observable(s) A at time T to a relative error ϵ .

In order to ensure that we have a known solution, we use an integrable model as our starting Hamiltonian. For example, we can consider the 1-dimensional transverse field Ising model (open boundary conditions):

$$H = \sum_{i=1}^{n-1} J_i Z_i Z_{i+1} + \sum_{i=1} h_i X_i$$
 (A1)

For concreteness we can take $J_i=-1$ and $h_i=-1$. For our initial state we can take the state $|++\cdots+\rangle$ where $X|+\rangle=|+\rangle$ and $X|-\rangle=-|-\rangle$. This state is stabilized by the set $X_1,X_2,...,X_n$. We can define a set of observables $A_{ij}=Z_iZ_j$ such that we can calculate the expectation value of these operators at time T efficiently by mapping the problem to a free fermion problem.

Our aim now is to obfuscate the initial state, the Hamiltonian, and the observables. Applying a random Clifford circuit to all three is not enough because it preserves the dimension of the dynamical Lie Algebra, which only scales polynomially with system size for this problem. We therefore propose to first apply a small number of T-gates followed by a random Clifford circuit. Our initial analysis indicates that even applying a single T-gate is enough to ensure that the dynamical Lie Algebra scales prohibitively. Some issues we are aware of:

- The weight of the terms in the obfuscated problem is larger than the weight of the operators in our application problem classes, which naively suggests it is a harder dynamics problem. Generating Clifford circuits that maintain a weight of 2 and obfuscate the problem, if possible, will require a more sophisticated strategy.
- We are not currently aware of an algorithm that can efficiently identify the integrable model that we have obfuscated. The algorithm in [30] is only able to identify the Z₂ symmetry of the model but not identify the original Hamiltonian. It is, however, possible that the algorithm that breaks our obfuscation would be discovered.

2. Open system

In this section, we outline a toy problem with a known solution that can be used to test an open system simulation of any size. We suggest reproducing the results of [18]. The specific details are below:

$$H = \sum_{i=1}^{n-1} J_i \sigma_i^z \sigma_{i+1}^z + \sum_{i=1}^{n-1} h_i \sigma_i^x$$
 (A2)

The values $J_i = J = 1.5$ and $h_i = h = 1$ are chosen. The system is also attached to two baths of different characteristics, given by the following Lindblad generators:

$$L_1 = \frac{1}{2}\sqrt{\Gamma_L^-}\sigma_1^-, \quad L_2 = \frac{1}{2}\sqrt{\Gamma_L^+}\sigma_1^+,$$
 (A3)

$$L_3 = \frac{1}{2} \sqrt{\Gamma_R^-} \sigma_n^-, \quad L_4 = \frac{1}{2} \sqrt{\Gamma_R^+} \sigma_n^+.$$
 (A4)

The rates are $\Gamma_L^-=1,~\Gamma_L^+=0.6,~\Gamma_R^-=1,~\Gamma_R^+=0.3.$ The task is to simulate the open system evolution of this system.

The initial state is all $|0\rangle$ state, and the evolution time needs

to be larger than the inverse of the gap of the Liovillian above, which is known to be $\approx 10.9 n^{-3}$.

The observables of interest are energy current and spin current. If the chain Hamiltonian is presented as a sum of local terms $H=\sum_m H_m$, the energy current is $Q_m=i[H_m,H_{m+1}]$, and the spin current $S_m=i[\sigma_m^z,H_m+H_{m-1}]$. The average energy and spin current are given as follows

$$S = \frac{1}{n-1} \sum_{m} S_m \tag{A5}$$

Their target values for different system sizes and chain locations are given in [18]. The energy current saturates at 0.35, while the spin current is at 0.12, with a uniform profile in the bulk of the system, corresponding to the ballistic transport.

While these models, as well as a large collection of other models that can be mapped to free fermions, have an efficient classical solution, it is a fair estimate of the resources required to solve actual application problems. The main differences in applications are higher dimensionality, a larger number of fermion bands, and the presence of interaction terms quadratic in fermionic operators. Our application instances range between 2000 and 15000 problem qubits, with 2000 to 3000 Lindblad terms. A successful quantum simulation of the n=15000 qubit benchmark would indicate that the benchmarked device has sufficient capabilities to contribute to application scenarios of MagLab and MIT search as well.